Enthalpy-based Thermal Evolution of Loops: II. Improvements to the Model

P. J. Cargill[1,2], S.J. Bradshaw[3] and J.A. Klimchuk[4]

1. Space and Atmospheric Physics, The Blackett Laboratory, Imperial College, London SW7 2BW (p.cargill@imperial.ac.uk)
2. School of Mathematics and Statistics, University of St Andrews, St Andrews, Scotland KY16 9SS
3. Department of Physics and Astronomy, Rice University, Houston, TX 77005
4. NASA Goddard Space Flight Center, Solar Physics Lab., Code 671, Greenbelt, MD 20771

Abstract

This paper further develops the zero-dimensional (0D) hydrodynamic coronal loop model "Enthalpy-based Thermal Evolution of Loops" (EBTEL) originally proposed by Klimchuk et al (2008), which studies the plasma response to evolving coronal heating. It has typically been applied to impulsive heating events. The basis of EBTEL is the modelling of mass exchange between the corona and transition region and chromosphere in response to heating variations, with the key parameter being the ratio of transition region to coronal radiation. We develop new models for this parameter that now include gravitational stratification and a physically motivated approach to radiative cooling. A number of examples are presented, including nanoflares in short and long loops, and a small flare. It is found that while the evolution of the loop temperature is rather insensitive to the details of the model, accurate tracking of the density requires the inclusion of our new features. In particular, we are able to now obtain highly over-dense loops in the late cooling phase and decreases to the coronal density arising due to stratification. The 0D results are compared to a 1D hydro code (Hydrad). The agreement is acceptable, with the exception of the flare case where some versions of Hydrad can give significantly lower densities. This is attributed to the method used to model the chromosphere in a flare. EBTEL is suitable for general use as a tool for (a) quick-look results of loop evolution in response to a given heating function and (b) situations where the

modelling of hundreds or thousands of elemental loops is needed. A single run takes a few seconds on a contemporary laptop.

**1. Introduction**.

Since the recognition in the 1970s that the magnetically confined solar corona is comprised of discrete loops, a great deal of effort has been devoted to modelling the temporal evolution of loop plasma. One approach is to solve numerically the one-dimensional hydrodynamic (1D hydro) equations of mass, momentum and energy conservation along a magnetic field line (or strand, or loop) in response to an imposed time-dependent heating function representing a flare or smaller heating event (e.g. Peres, 2000). Of importance is the ability of such models to generate "observables" that can be used to interpret coronal data (e.g. Bradshaw and Cargill, 2006; Bradshaw and Klimchuk, 2011).

1D hydro models have two difficulties. One is the optically thick chromosphere at the lower boundaries. In principle this requires a full radiative-hydrodynamic treatment (e.g. McClymont and Canfield, 1983a,b) but one can attach a simple lower atmosphere that preserves the essential physics (e.g. Klimchuk et al., 1987; Antiochos et al., 1999). The second, and more significant, difficulty is the limitation imposed on the computational timestep by thermal conduction in the transition region (hereafter TR). In static equilibrium loops (e.g. Martens, 2010) the downward heat flux implies a temperature scale height ($L_T$) of under 1 km in the TR, and even shorter in hot flaring loops. Resolving this requires a fine grid, but when modelling thermal conduction the timestep scales as the smallest value of $L_T^2$, implying long run times.

There is thus a need for simple and fast ways of modelling the coronal response to time-dependent heating. "Zero-dimensional" (0D) models, which average over the loop's spatial dimension (Kuin and Martens, 1982, Fisher & Hawley, 1990, Kopp and Poletto, 1993, Cargill, 1994, Klimchuk et al., 2008, Aschwanden and Tsiklauri, 2009) accomplish this. In addition to providing "quick look" results, 0D models are useful if a loop is comprised of many hundreds or thousands of thin, thermally isolated, randomly heated strands (Cargill, 1994), which conventional 1D hydro modelling still finds a large task.

The success of 1D and 0D models depends on handling correctly the exchange of matter between the corona, TR and chromosphere in response to a changing coronal

temperature. While the above 0D models all address this to varying degrees (see Cargill et al., 2011, hereafter Paper 3), we base our discussion here on the work of Klimchuk et al., (2008: hereafter Paper 1). In Paper 1 we developed a 0D model whose centrepiece was the explicit calculation of the enthalpy flux to and from the corona. The model, called EBTEL: "Enthalpy Based Thermal Evolution of Loops", divides a loop into coronal and TR parts, the boundary being defined as where thermal conduction changes from a loss to a gain. Whether the enthalpy flux is into, or out of, the corona depends on whether the TR can radiate away the downward heat flux. If it cannot do this, then material is "evaporated" into the corona, whose density then increases (e.g. Antiochos and Sturrock, 1978). If the TR radiation cannot be powered by the downward heat flux, then there is a downward enthalpy flux, and the coronal density decreases (e.g. Cargill et al., 1995). The model was compared with several 1D hydro simulations of an impulsively heated loop (starting each time with the same initial conditions), and gave reasonable agreement.

EBTEL relies on three parameters, the most important of which is the ratio of the TR to coronal radiative losses. They govern both the initial equilibrium and how the loop cools after impulsive heating. It has become apparent through use of EBTEL, and attempts to benchmark EBTEL results against other known solutions of loop cooling, that the choice of this parameter in Paper 1 may only be appropriate for a long, tenuous loop. Thus, this paper seeks to put the EBTEL model on a firmer foundation and also looks at a broader range of loop evolution. The physical principles are unchanged, but we have undertaken a re-evaluation of the three key parameters (Section 2). The result is a model that now can follow with a good degree of accuracy, when compared with a 1D hydro code, the evolution of loops over a wide range of lengths and temperatures (Section 3). In Paper 3 we will provide a comparison of 0D models and sources of potential discrepancy with 1D models.

## 2. The models

### 2.1 The governing equations of EBTEL

The details of the model are discussed in Paper 1 and are restated briefly here. The 1D energy equation is:

$$\frac{\partial E}{\partial t} = -\frac{\partial}{\partial s} v(E + p) - \frac{\partial F_c}{\partial s} + Q - n^2 \Lambda(T) \qquad (1)$$

where v is the velocity, $E = \frac{p}{\gamma - 1}$, $F_c = -\kappa_0 T^{5/2} \frac{\partial T}{\partial s}$ is the heat flux, $Q(t)$ is a heating

function that includes both steady and time-dependent components, $\Lambda(T) = \chi T^\alpha$ is the

radiative loss function in an optically thin plasma as defined in Paper 1, Equation (3),

and $s$ is a spatial coordinate along the magnetic field. We have assumed that the flow

is always subsonic and that gravity can be neglected from the viewpoint of the

energetics. There is also an equation of state $p = 2nkT$.

For a corona loop of half-length $L$ and a transition region of thickness $l$ (<<$L$), we

define the boundary between corona and TR as the location where conduction

changes from a loss to a gain (Vesecky et al., 1979). Integrating Eq (1) from the top of

the TR to the top of the loop and enforcing symmetry boundary conditions, we find:

$$\frac{L}{\gamma - 1} \frac{d\bar{p}}{dt} = \frac{\gamma}{\gamma - 1} p_0 v_0 + F_0 + L\bar{Q} - R_c \qquad (2)$$

where "overbar" denotes an averaged coronal quantity, subscript "0" denotes a

quantity at the base of the corona (or top of the TR) and $R_c = \bar{n}^2 \Lambda(\bar{T})L$. Note that the

heat flux and enthalpy flux play equivalent roles in providing energy to the TR.

Integrating over the TR, and assuming the heat flux and flow vanish at its base, the

pressure derivative and the heating can be eliminated since $l << L$, giving:

$$\frac{\gamma}{\gamma - 1} p_0 v_0 + F_0 + R_{tr} = 0 \qquad (3)$$

where $R_{tr}$ is the integrated radiative TR losses. Eq (3) can then be combined with Eq

(2) to give an equation for the coronal evolution:

$$\frac{1}{\gamma - 1} \frac{d\bar{p}}{dt} = \bar{Q} - \frac{1}{L}(R_c + R_{tr}) \qquad (4)$$

Note that conduction does not appear in Eq (4) emphasising its role as an energy

redistribution mechanism as opposed to an energy loss. To calculate the density

evolution, we adopt a similar approach to the mass equation, and in the corona find:

$$\frac{d\bar{n}}{dt} = \frac{n_0 v_0}{L} = -\frac{\gamma - 1}{2kT_0 L\gamma}(F_0 + R_{tr}). \qquad (5)$$

The average coronal temperature then follows from the equation of state:

$$\frac{1}{\overline{T}}\frac{d\overline{T}}{dt} = \frac{1}{\overline{p}}\frac{d\overline{p}}{dt} - \frac{1}{\overline{n}}\frac{d\overline{n}}{dt} \tag{6}$$

To solve the set of coronal equations (4) – (6) for the primary variables $\overline{T}$, $\overline{n}$ and $\overline{p}$, we need to define $R_{tr}$, $T_0$ and $F_0$ in terms of the coronal quantities. The conductive losses are defined in terms of the loop apex temperature $(T_a)$: $F_0 = -(2/7)\kappa_0 T_a^{7/2}/L$ (Paper 1: Eq 20), so that there are three temperatures that characterise the corona: $\overline{T}$, $T_a$ and $T_0$. $T_a$ and $T_0$ are defined in terms of the primary variable $\overline{T}$ as $C_2 = \overline{T}/T_a$, $C_3 = T_0/T_a$. Finally, we define a third parameter: $C_1 = R_{tr}/R_c$ which modifies Eqs (4) and (5) to:

$$\frac{1}{\gamma-1}\frac{d\overline{p}}{dt} = \overline{Q} - \frac{R_c}{L}(1+C_1) \tag{7}$$

$$\frac{d\overline{n}}{dt} = \frac{n_0 v_0}{L} = -\frac{C_2}{C_3}\frac{(\gamma-1)}{2k\overline{T}L\gamma}(F_0 + C_1 R_c) \tag{8}$$

Specification of $C_{1-3}$ is then required to solve Eq (6), (7) and (8).

## 2.2 Modifications to the EBTEL model

The original version of EBTEL described in Paper 1 used constant values of $C_{1-3}$. However, as EBTEL has become more widely used, it is clear that further analysis of $C_{1-3}$ is required. Here we want to address three questions: (i) are the "baseline" values used in Paper 1 correct? (ii) how can EBTEL handle stratification due to gravity in long loops and (iii) how does EBTEL handle loop cooling when radiative losses strongly dominate? A secondary issue is how a general radiative loss function with a multiple power law can be included. We will show that these questions can be addressed by adopting a variable $C_1$ within any given loop study, while implementing minor changes to $C_2$ and $C_3$. $C_1$ is the most important parameter because the TR radiation regulates the value of the heat flux or enthalpy flux out of the corona that powers it, which in turn feeds into the coronal density and temperature.

### 2.2.1 Assessment of parameters: equilibrium loops

Paper 1 used static equilibrium loop solutions to calculate $C_{1-3}$. This is likely to be valid around the time of peak density when coronal radiative and conductive losses are comparable. Two approaches were considered. One had fixed values for all temperatures, namely $C_1 = 4$, $C_2 = 0.87$ and $C_3 = 0.5$, and this was used to produce all the Figures in Paper 1. The second used a polynomial fit for $C_1$ and $C_3$ over the temperature range $1 - 10$ MK based on solutions of the equilibrium energy equation (Tables 1 and 2 of Paper 1). However the values of $C_1$ and $C_3$ quoted for short loops and $T > 3$ MK (Table 1 of Paper 1) are incorrect, and so the polynomial fit for $C_1$ and $C_3$ present in early versions of the publicly available EBTEL code should not be used.

We now reassess $C_{1-3}$ for static loops. First we use a simple power law radiative loss function and defer to Section (c) below how to include a multiple power law. We use the approximation $\Lambda(T) = \chi T^{\alpha} = 1.95 \ 10^{-18} \ T^{-2/3}$ as our baseline power law, modified to $\Lambda(T) = 1.1 \ 10^{-31} T^{2}$ below $10^{5}$ K to avoid unrealistic losses at low temperatures. To calculate hydrostatic thermal equilibrium numerically, a Runge-Kutta method is used. $T_a$ and $L$ are specified, and a double iteration calculates the base pressure and (constant) heating such that the appropriate boundary conditions are satisfied ($T = T_a$ and $dT/ds = 0$ at top of loop) for a given base temperature and vanishing base heat flux. This gives the familiar scaling laws between $T_a$, $L$, $Q$ and $p_0$.

The derivation of $C_{1-3}$ for general equilibrium loops relies on first calculating values for loops with no gravity and for a single power law form of $\Lambda(T)$. The details of this are presented in Appendix A. There we first use the work of Martens (2010) to demonstrate analytically that $C_1$ and $C_3$ are independent of all parameters except the slope of the radiative loss function for the case with no low temperature correction to $\Lambda(T)$. Modifying $\Lambda(T)$ at low temperatures shows that in the absence of gravity, $C_{1-3}$ may be taken as constants over a wide range of temperature and length (and hence pressure and heating rate). For $L = 2.5$, 5 and $7.5 \ 10^{9}$ cm and $T_a$ between 0.5 - 10 MK, $C_2$ and $C_3$ are roughly constant with values of 0.9 and 0.6 respectively. $C_1$ varies a little more with $T_a$, but can be taken as approximately 2. We propose these as the "baseline" values of the constants and now discuss how they are modified to include other effects for equilibrium loops.

**(a) Gravity:** Here the main effect is that, while the TR radiation is driven by the downward heat flux, and so for a given coronal temperature is roughly fixed, the coronal radiation falls due to the stratification. Thus larger values of $C_1 = R_{tr}/R_c$ can be expected for loops with significant values of the ratio $\lambda/L$, where $\lambda = c_s^2/g = (2kT_a/m_p)/g$ is the gravitational scale height. We have thus solved the hydrostatic equations using the simple power law loss function for two loop lengths: 5 x $10^9$ and 7.5 x $10^9$ cm and temperatures between 5 x $10^5$ and 4 x $10^6$ K. In the upper panels of Figure 1, the stars denote $C_1$ when gravity is absent (around 2 in all cases) and the circles $C_1$ when gravity is included. [Note that static solutions for $T_a = 5$ x $10^5$ K with $L = 7.5$ $10^9$ cm could not be found: see also Serio et al., 1981.] $C_1$ increases as the temperature and scale height decrease. Note that for the loop shown in Figure 1 of Paper 1 ($T_a = 2$-$3$ *MK*, $L = 7.5$ $10^9$ cm), $C_1 = 4$ seems reasonable.

We now seek a parameterisation of the form $C_1(T, L)$. There is little dependence of $C_1$ on loop length itself, rather the key parameter is the ratio $L/\lambda$. We write:

$$C_1 = \frac{R_{tr}}{R_c} = \left[\frac{R_{tr}}{R_{tr}(g=0)}\right]\left[\frac{R_{tr}(g=0)}{R_c(g=0)}\right]\left[\frac{R_c(g=0)}{R_c}\right] \tag{9}$$

where quantities labelled "$g=0$" are values when gravity is neglected. The lower panels of Figure 1 shows the ratios $R_{tr}(g=0)/R_{tr}$ (stars) and $R_c(g=0)/R_c$ (circles) as a function of $T_a$. The TR ratio is roughly unity which can be explained by noting that in static equilibrium, the energy balance in the TR is between the downward heat flux from the corona and the TR radiation [Eq (3)]. For given $L$ and $T_a$, the heat flux is roughly the same irrespective of whether the corona is stratified or not, so the TR radiation must also be roughly the same. The coronal ratio shows the expected drop in radiation when gravity is included. Now the second ratio in (9) is known to be 2, so if we have a simple expression for the third, we can calculate $C_1$ for different stratified loops. We argue that, for a given coronal temperature,

$$\frac{R_c(g=0)}{R_c} \approx \frac{\left(\overline{n}^2\overline{T}^\alpha\right)_{g=0}}{\overline{n}^2\overline{T}^\alpha} \approx \frac{\left(\overline{n}^2\right)_{g=0}}{\overline{n}^2} \approx \frac{p_0^2}{p^2} \tag{10}$$

assuming the coronal length is the same with and without gravity and the averages are as defined in Paper 1, Eq (11).

8

Next assume that the coronal pressure is given by: $p(s) \approx p_0 \exp\left[-\dfrac{2L}{\pi\bar{\lambda}}\sin\left(\dfrac{\pi s}{2L}\right)\right]$ for a semi-circular loop where we use a scale height based on the average temperature ($\bar{T} = C_2 T_a$) and that hydrostatic density stratification occurs only in the corona. We have calculated the average pressure by integrating $p(s)$ numerically and find that this average value is well approximated by using the actual pressure at $s/L = 0.4$. So, the average pressure is written as: $\bar{p} = p_0 \exp(-2L\sin(\pi/5)/\bar{\lambda}\pi)$ to finally give:

$$C_1 = \frac{R_{tr}}{R_c} = \frac{R_{tr}(g=0)}{R_c(g=0)}\exp(4L\sin(\pi/5)/\bar{\lambda}\pi). \tag{11}$$

The plus signs in the upper panels of Fig 1 show that these values of $C_1$ work reasonably well for all but the lowest temperature.

**(b) Multiple power law radiative loss function:** Next, neglecting gravity, we evaluate $C_1$ for a more complicated loss function by comparing results for the EBTEL loss function and the single power law one:

$$C_1 = \frac{R_{tr}}{R_c} = \left[\frac{R_{tr}(T)}{R_{tr}(\alpha=-2/3)}\right]\left[\frac{R_{tr}(\alpha=-2/3)}{R_c(\alpha=-2/3)}\right]\left[\frac{R_c(\alpha=-2/3)}{R_c(T)}\right] \tag{12}$$

where $R_{tr}(T)$ and $R_c(T)$ evaluate the loss functions at a given temperature using the full power law in EBTEL. The right hand plot in Figure 2 shows little difference in the TR losses between the two radiative loss models (stars), so we can assume the first term in (12) is unity. The explanation is once again that the TR losses are determined by the heat flux from the corona. The coronal loss (circles) does show differences between the models. The second term in (12) is 2. For the third term, we can use the average coronal temperature ($T = \bar{T} = C_2 T_a$) in Eq (12) to evaluate the radiation. The left hand plot of Figure 2 shows the same quantities as the lower panels of Figure 1 for a loop of length $5\ 10^9$ cm. This model for $C_1$ is almost independent of the loop length.

**(c) Gravity and multiple power law loss function.** We now combine the two corrections for loops with gravity and the general EBTEL loss function by replacing the ratio before the exponential in Eq (11) (which has no gravity and the simple loss function) with Eq (12) (which has no gravity and the full loss function), and using the fact that the TR losses are roughly the same for all cases:

$$C_1(eq) = \frac{R_{tr}(g,\overline{T})}{R_c(g,\overline{T})} = \left[\frac{R_{tr}(g=0,\alpha=-2/3)}{R_c(g=0,\alpha=-2/3)}\right]\left[\frac{R_c(g=0,\alpha=-2/3)}{R_c(g=0,\overline{T})}\right]\exp(4L\sin(\pi/5)/\overline{\lambda}\pi)$$

$$(13)$$

where we now denote the "equilibrium" value of $C_1$ as $C_1$(eq). The first ratio will be taken as 2 in this paper, but is written in a general form to allow for changes to the coronal losses that no longer use our power law approximation. Figure 3 shows the results in the same format as Figure 1 for two temperature ranges and a loop length of $5\ 10^9$ cm. Other than at very low temperatures, (13) does acceptably.

## 2.2.2 Radiative cooling phase

Equilibrium conditions are a good approximation if the strand (or loop) is evolving slowly, but may not be if it evolves rapidly. Consider a nanoflare event. The strand is far from equilibrium during the impulsive heating and the start of the thermal conduction cooling phase that follows. TR radiation is energetically insignificant at this time, so $C_1$ does not affect the evolution. Static equilibrium is a reasonable approximation during the next phase of cooling when both thermal conduction and radiation, and possibly also enthalpy, are important. However, during the final phase of cooling when either radiation or enthalpy dominates, the equilibrium value of $C_1$ is a poor approximation.

It is well known that for short, hot loops, there is a scaling $T \sim n^{2\,-\,2.5}$ during radiation-dominated cooling (Serio et al., 1991; Cargill et al., 1995; Bradshaw and Cargill, 2005, 2010a,b), with a scaling approaching $T \sim n$ for longer, more tenuous loops (Bradshaw and Cargill, 2010b). We can use the EBTEL equations adapted to radiative cooling to determine the appropriate value of $C_1$. In the absence of gravity and neglecting thermal conduction and heating, Eq (4) and (5) are:

$$\frac{1}{\gamma-1}\frac{d\overline{p}}{dt} = -\frac{1}{L}(R_c+R_{tr}), \quad \frac{d\overline{n}}{dt} = -\frac{(\gamma-1)R_{tr}}{2kT_0L\gamma} \tag{14}$$

and so, on writing $T \sim n^\delta$ we can relate $T$ and $n$ as follows:

$$\delta+1 = \frac{1}{p}\frac{dp}{dt} \div \frac{1}{n}\frac{dn}{dt} = \gamma\frac{T_0}{T}\frac{(R_c+R_{tr})}{R_{tr}} = \gamma\frac{C_3}{C_2}\frac{(1+C_1)}{C_1} \tag{15}$$

This can be solved for $C_1$ as:

$$C_1(rad) = \left( \frac{C_2(1+\delta)}{\gamma C_3} - 1 \right)^{-1} \qquad (16)$$

where $T_0$ is now the temperature at which enthalpy changes from a loss to a gain (Bradshaw and Cargill, 2010a,b) and we denote $C_1(rad)$ as the value of $C_1$ in the radiative phase. For $\delta = 2(1)$, and the same values of $C_2$ and $C_3$ as for equilibrium loops, we find $C_1 = 0.59(1.25)$. Bradshaw and Cargill (2010b) suggest that $\delta$ can be even larger for small loops, in the range $2.3 - 2.4$ which gives $C_1(rad) = 0.5$. We chose this as the baseline value for the radiative phase in the absence of gravity and $\alpha = -2/3$.

To include gravity and a full $\Lambda(T)$, we adopt the same approach as in Section 2.2.1 on the basis of our work on radiative cooling (Cargill et al., 1995; Bradshaw and Cargill, 2005, 2010a,b):

$$C_1(rad) = \frac{R_{tr}}{R_c} = 0.5 \left[ \frac{R_c(g=0, \alpha=-2/3)}{R_c(g=0, \bar{T})} \right] \exp(4L\sin(\pi/5)/\bar{\lambda}\pi). \qquad (17)$$

Thus, including gravity increases $C_1$ corresponding to the decrease in $\delta$ discussed in Bradshaw and Cargill (2010b).

### 2.2.3 Overall implementation of $C_1$

We now wish to implement a formalism for $C_1$ that takes on the equilibrium value when conductive and radiative losses are of the same order, and the radiative value when conduction is unimportant. We define the density for equilibrium conditions as $n_{eq}$, and note that conductive (radiative) cooling of an impulsively heated loop at a given temperature is characterized by $n < (>) n_{eq}$ (e.g. Cargill, 1994, Cargill and Klimchuk, 2004). A formula of the generic form $C_1 = F(n/n_{eq})$ is considered, and we require $C_1 = C_1(eq)$ when $n/n_{eq} = 1$ and $C_1 = C_1(rad)$ when $n/n_{eq}$ is large. We define an "equilibrium" loop to be one where the coronal conductive loss is twice the coronal radiative loss ($C_1 = 2$). The following form of $F$ is considered:

$$C_1 = F(n/n_{eq}) = \frac{C_{c0} + C_1(rad)(n/n_{eq})^m}{1 + (n/n_{eq})^m}, \qquad (18)$$

where $m$ is taken to be 1 or 2. $C_{c0}$ is the "conductive" value of $C_1$ and is adjusted to give $C_1 = C_1(eq)$ for $n = n_{eq}$. One thus gets:

11

$$C_{c0} = 2C_1(eq) - C_1(rad),$$

so, for $C_1(eq) = 2$, $C_1(rad) = 0.5$ we get $C_{c0} = 3.5$.

The quantity $n_{eq}$ can be obtained from the EBTEL equations in terms of the loop temperature and density:

$$n_{eq}^2 = \frac{2\kappa_0}{7C_1(eq)\Lambda(\overline{T})L^2}\left(\frac{\overline{T}}{C_2}\right)^{7/2}$$

One can then write

$$\left(\frac{n}{n_{eq}}\right)^2 = \frac{\tau_c}{\tau_R}$$

where $\tau_c$ and $\tau_R$ are the instantaneous conductive and radiative cooling times, defined as $\tau_c = \frac{21k\overline{n}L^2 C_2}{2\kappa_0}\left(\frac{C_2}{\overline{T}}\right)^{5/2}$, $\tau_R = \frac{3k\overline{T}C_1(eq)}{\overline{n}\Lambda(\overline{T})}$, to give an alternative form of Eq (18):

$$C_1 = \frac{C_{C0} + C_1(rad)(\tau_c/\tau_R)^{m/2}}{1 + (\tau_c/\tau_R)^{m/2}} \tag{19}$$

### 2.2.4 The Differential Emission Measure

In Paper 1 we calculated separate coronal and transition region differential emission measures (DEMs), the latter by two distinct methods. The DEM is defined as: $DEM(T) = n^2(\partial T/\partial s)^{-1}$. Our modifications to EBTEL do not change the way the coronal DEM is calculated since the coronal parameters are our primary variables. On the other hand, the TR DEM relies on an assumption of constant pressure in the loop, which the introduction of gravity will invalidate. In Paper 1 we calculate the DEM by solving the following quadratic equation for $\partial T/\partial s$:

$$\kappa_0 T^{3/2}\left(\frac{\partial T}{\partial s}\right)^2 - 5kJ_0\left(\frac{\partial T}{\partial s}\right) - \left(\frac{p_{TR}}{2kT}\right)^2 \Lambda(T) = 0$$

While $J_0$ is constant and determined by the mass flow to and from the corona, the pressure in the last term is a TR quantity. Thus, when gravity is important we need to modify this term to account for the fact that the TR pressure will be larger than the coronal one. This is done by using our coronal pressure modification in reverse, so we write $p_{TR} = \overline{p}\exp(2L\sin(\pi/5)/\overline{\lambda}\pi)$. This feature is demonstrated in the next Section.

12

In Paper 1 we also provided approximate forms of the DEM for three cases of loop evolution: strong conduction-driven evaporation, equilibrium, and strong radiative-driven condensation (draining). Of these, the third is unmodified, while the first two both involve the TR pressure, and need to be changed accordingly.

## 2.3 The Hydrad Code

An important part of our work is a comparison of the EBTEL results with the 1-D Hydrad code. This code has been fully documented in Bradshaw and Mason (2003a,b) so that we summarise the details briefly here. Hydrad solves separate time-dependent electron and ion energy equations together with equations of mass and momentum conservation and an equation of state. For the EBTEL comparison, we introduce an anomalously high electron-ion collision frequency that ensures $T_i = T_e$ under all conditions. For radiative losses, we supress the full capability of Hydrad to track multiple ion species, and use the same optically thin loss function as in EBTEL.

In the figures, we show Hydrad results averaged over the top 80% of the loop. With the exception of the long loop (Case 3 below), there is little difference in the average $T$ and $n$ when the top 10, 50 or 80% of the loop is considered. For long loops the 80% average gives a density 25% larger than the 10% one, which can be attributed to the gravitational stratification present.

## 3 Results

We present four examples of loop heating. Each case is characterised by: (i) a loop half-length $L$, (ii) a background heating function which in turn implies a pre-event temperature and density, and (iii) a flare or nanoflare heating function with the form of a triangular pulse. Both the background heating and flare/nanoflare heating are uniform in space.

### 3.1 Nanoflare heating of a short loop

13

The first case is a nanoflare in a short loop. A heating pulse with a half-width of 100 sec and peak magnitude $10^{-2}$ ergs $cm^{-3}$ $s^{-1}$ is released in a loop with half-length 25 Mm. This has a total energy release of 2.5 $10^9$A ergs $cm^{-2}$, where A is the loop cross-sectional area. For a strand diameter of 200 km, we get a release of $(\pi/2) \times 10^{24}$ ergs. The background heating is $10^{-5}$ ergs $cm^{-3}$ $s^{-1}$ giving an initial temperature and density of 0.53 MK and 1.3 $10^8$ $cm^{-3}$ respectively.

For clarity we show the new developments with EBTEL in two consecutive plots. The four panels of Figure 4 show the loop temperature and density as a function of time (top left and top right), the relationship between $T$ and $n$ (lower left) and $C_1$ (lower right), for cases where neither gravitational nor radiative loss corrections are included in $C_1$. The plots show: (i) the EBTEL-1 results ($C_1 = 4$, $C_2 = 0.89$, $C_3 = 0.5$: dots), (ii) the new "fixed" constant values ($C_1 = 2$, $C_2 = 0.9$, $C_3 = 0.6$: dash-dot), (iii) the Hydrad simulation (thick solid), (iv) the linear $C_1$ profile ($m = 1$ in Eq (18), dashed) and (v) the quadratic $C_1$ profile ($m = 2$ in Eq (18), thin solid). The small panel in the temperature plot shows the evolution around the maximum.

We start by noting that the temperature evolution for all the methods is broadly similar. $C_1$ has little influence on the peak temperature since radiation is not playing any significant role at that time: the peak arises from a balance between heating and thermal conduction. EBTEL-1 has the lowest peak temperature (3.86 MK), followed by Hydrad (3.95 MK) and then EBTEL-2 (4.13 MK). The various models have slightly different initial densities for the same background heating which will have a small influence on the peak temperature. It can also be seen that after the decay phase there is a temperature undershoot for the quadratic $C_1$ model as it tries to recover the initial equilibrium.

On the other hand, the density profiles do depend on the method used. EBTEL-1 has the lowest peak density of the EBTEL runs (1.1 $10^9$ $cm^{-3}$) and peaks soonest. If we compare this with $C_1 = 2$ which peaks at 1.17 $10^9$ $cm^{-3}$, the larger value of $C_1$ requires the corona to lose more energy both by conduction and, more precisely, reduces the enthalpy transfer to the corona (the transition region radiation is stronger and can accommodate more of the heat flux). The two non-uniform models of $C_1$ fall between

14

the first two cases. Hydrad gives a lower peak density of $10^9$ cm$^{-3}$ and has oscillations due to material sloshing back and forward in the loop in response to the heating.

The density in the decay phase shows more striking differences. Using a constant value of $C_1 = 2$ increases the density and gives a (fortuitous, as we shall see) agreement with Hydrad. The linear and quadratic models increase the density further, with the discrepancy of the quadratic model being the more significant. The *T-n* scalings in the decay phase are also informative. To help the eye in this panel we include two thin solid lines showing $T \sim n^{1/2}$ (equilibrium) and $T \sim n^2$ (radiative cooling) scalings. $C_1 = 4$ gives a *T-n* scaling corresponding to an "equilibrium" loop and examination of the losses from the corona due to conduction and radiation show that they are indeed equal after a few hundred seconds. A constant $C_1 = 2$ does not give the expected *T-n* scaling in the radiative phase. The non-uniform $C_1$ models give the *T-n* scalings that are closer to what is expected, with the quadratic profile giving the faster transition and a clearly over-dense loop. The Hydrad simulation gives a shallower slope in the *T-n* relation.

However, just including a variable $C_1$ to account for radiative cooling is not the whole story. In Figure 5 we explore the effect of including the corrections due to gravity and the multiple power law $\Lambda(T)$. The figure has the same format as Figure 4, but we now show EBTEL-2 results using (i) the quadratic $C_1$ (dotted), (ii) the correction to the quadratic case due to the full loss function (dash-dot), (iii) the correction due to gravity and the loss function for the quadratic profile (solid), linear profile (dashed) and the Hydrad results (thick solid). The radiative correction does not make a major difference, but the gravity correction does. The peak density moves slightly closer to the Hydrad value, but the agreement in the decay phase, where gravity becomes important, improves. The two models for $C_1$ straddle the Hydrad solution, with the linear profile slightly low, and the quadratic one slightly high.

The changes introduced by gravity can also be seen in the $C_1$ plot. Coronal stratification is sufficiently important ($L/\lambda$ of order 0.4 or more after 1000 sec) that in the radiative phase one moves back towards values of $C_1$ more typical of equilibrium loops rather than the small values typical of radiative cooling in flare loops.

In Paper 3 we discuss more fully the fact that getting a reasonable answer for the density in 0D models is much harder than the temperature, the radiative phase in particular being awkward. We thus feel that the agreement in the density between EBTEL-2 and Hydrad shown here is satisfactory. This is only achieved by using a model for $C_1$ that evolves in time and includes gravitational stratification. Finally, the fact that the linear and quadratic $C_1$ models straddle the Hydrad result means we cannot yet comment on the preference of one over the other.

Figure 6 shows the DEMs for some of these cases. These are computed over the 5000 secs of the run, and so are averages over the life of the strand. On the left, the coronal DEM is shown for four runs: original EBTEL (dash-dot), quadratic $C_1$ profile (dotted) and quadratic and linear $C_1$ modified for gravity (solid and dashed). The thick dashed line shows the TR DEM for the gravitationally modified quadratic profile. In fact, for this case the gravitational correction to the TR DEM makes little difference. On the right are the total (corona + TR) DEMs for EBTEL-1 (dash-dot), EBTEL-2 with corrections (solid) and Hydrad (thick solid). All the EBTEL models give reasonable agreement with Hydrad above 1.5 MK as would be expected from the previous figures. Below that temperature, the coronal value from EBTEL-1 falls significantly compared to the EBTEL-2 results. However, when the TR part is included, the total DEM for both EBTEL models compares well with Hydrad: the only feature of note is a small depression in the EBTEL-1 DEM compared the Hydrad and EBTEL-2 around 1 MK.

## 3.2 Nanoflare heating of a long loop

The second case re-examines the long, tenuous loop discussed in Paper 1. The loop has a half-length of 7.5 $10^9$ cm and is heated by a nanoflare with amplitude 1.5 $10^{-3}$ ergs cm$^{-3}$ s$^{-1}$ and half-width 250 secs. There is a background heating of 5 $10^{-6}$ ergs cm$^{-3}$ s$^{-1}$ giving an initial temperature and density of 0.52 MK and 3 $10^7$ cm$^{-3}$ respectively. When this example was presented in Paper 1, reasonable agreement with the 1-D hydro code ARGOS (Antiochos et al., 1999) was noted.

Figure 7 shows results in the same format as Figure 4 for: (i) EBTEL-1 (dash-dot), (ii) EBTEL-2 with quadratic density profile (dots), (iii) as (ii) with gravity and radiation correction for quadratic and linear $C_1$ profile (solid and dashed) and (iv) Hydrad (thick solid). In (iii) the radiative correction has a small influence. As in the first example, the temperature throughout shows little difference between the four runs whereas the density varies considerably. We see that the unmodified quadratic $C_1$ model gives very high densities in the decay phase that disagree significantly with the Hydrad and ARGOS results. However, modifying $C_1$ to include gravity gives a density that is closer to the EBTEL-1 model. The Hydrad density is lower than all the EBTEL runs, the discrepancy being smaller at peak density than in Paper 1. In the decay phase, the linear $C_1$ profile now does better than the quadratic one when the gravitational correction is included. Thus, we see that the agreement between EBTEL-1 and ARGOS in Paper 1 was partly coincidental. Interestingly the constant value of $C_1 = 4$ used in EBTEL-1 does very well for this example. If one draws a straight line at $C_1 = 4$ across the lower right panel, one could argue that this is indeed a reasonable first approximation to our variable $C_1$.

The DEMs are shown in Figure 8 in the same format as Figure 6. We see that inclusion of the quadratic $C_1$ profile introduces overdense loops and so increases the DEM below the peak temperature but introduction of the gravitational correction removes this and we recover something quite similar to that in Paper 1. There is a small pressure correction to the transition region DEM as shown by comparing the thick dashed (includes effect) and dot-dashed (omits effect) in the left panel.

## 3.3 Nanoflare with higher background heating

Both the previous examples had a nanoflare with energy much larger than the background thermal energy in the loop or, equivalently, the background heating is much smaller than the peak nanoflare heating. However, nanoflare heating is not necessarily confined to a single heating / cooling cycle in a loop. Evidence now suggests that impulsive heating on occasions may be occurring in loops or strands that have not undergone such a cycle (e.g. Warren et al, 2011), so that the heating takes place in a higher ambient density.

We have re-run the case described in Section 3.1 with a higher background heating. To conduct a proper comparison with Hydrad, care is needed in setting up the initial state. The reader will have noticed in the earlier figures that the initial density and temperature was different in Hydrad and EBTEL for the same background heating. [This is a reflection of the fact that modelling the full spatial structure of a loop will give a slightly different value of the temperature and density from an approximate model that neglects this structure.] So long as the nanoflare is "large" in the sense that at its peak intensity the heating is much stronger than the background, this does not matter. However, for a "weak" nanoflare, it is important to run EBTEL and Hydrad with roughly the same initial density. Thus, Hydrad is initialised with a background heating of $4.1 \times 10^{-4}$ ergs cm$^{-3}$ s$^{-1}$ giving a temperature and density of 1.36 MK and 8.31 $\times 10^8$ cm$^{-3}$ respectively. EBTEL has a heating of $3.93 \times 10^{-4}$ ergs cm$^{-3}$ s$^{-1}$ giving a temperature and density of 1.48 MK and 8.31 $\times 10^8$ cm$^{-3}$ respectively. To compare with EBTEL-1, we have to increase the background heating by 50% to ensure starting from roughly the same temperature and density. The nanoflare itself is as in Section 3.1.

Figure 9 shows the evolution of the temperature and density for EBTEL-1, EBTEL-2 with the gravitational and radiative corrections with both linear and quadratic $C_1$ profiles and Hydrad. The agreement between the two approaches can be considered satisfactory with the linear $C_1$ profile doing a better job with the density. Comparing with Figure 4, we see lower peak temperatures and, although the peak density is higher when the initial density is higher, the actual density increase is smaller. In the case of Section 3.1, the peak temperature is set by a balance between the maximum heating rate and thermal conduction losses. With the higher initial density we have here, the temperature never reaches this point. Instead, the peak temperature corresponds to an approximate equality between the total energy input of the nanoflare and the increase in thermal energy, $p/(\gamma-1)$, at roughly constant density.

**3.4 Small Flare**

Our fourth example is of a modest flare in a short loop with $L = 25$ Mm. The maximum heating is 2 ergs cm$^{-3}$ s$^{-1}$, and the pulse half-width 100 secs, so the total heating per unit area is $5 \times 10^{11}$ ergs cm$^{-2}$ which for a loop diameter 20% of the half-

18

length gives a total energy input of 4 $10^{29}$ ergs. We neglect "thick target" heating which was discussed in Paper 1 and remains part of the EBTEL code.

The four panels of Figure 10 show the loop temperature and density in the same format as above for the EBTEL-1 values, the various profiled versions of $C_l$ and two Hydrad runs. For this flaring case the gravitational correction to $C_l$ is not important. Once again, the temperature plots for all the approaches are superficially similar. Hydrad gives the highest temperatures and EBTEL-1 the lowest. The significant differences are seen in the density. The Hydrad density is much lower than all of the EBTEL runs: a peak of 2.5 $10^{10}$ from Hydrad contrasting with 4 $10^{10}$ from the various EBTEL runs. In the decay phase the differences narrow, but we see from the T-n plot that while the scaling between T and n in the Hydrad run is consistent with our expectations, the EBTEL runs have a weaker decay (i.e. T $n^{<2}$).

We have addressed the density discrepancy from a number of viewpoints that are discussed more fully in Paper 3. These include: the coronal pressure forcing the chromosphere downward, leading in turn to longer loops and lower coronal densities (Klimchuk, 2006) and the violation of the subsonic flow assumption. However, for this case, we believe that the low coronal density lies in the treatment of the chromospheric radiation in Hydrad. The baseline version of the code limits the radiative losses if the density above 30 kK exceeds $10^{12}$ cm$^{-3}$. This can be seen as modelling a number of processes, such as optically thick effects. The thick dashed line in Figure 10 shows what happens if this threshold density is set to $10^{11}$ cm$^{-3}$. Now there is much better agreement between EBTEL and Hydrad with the linear $C_1$ profile doing slightly better. The density limiter now does not permit the initial large downward heat flux to be radiated away at high density, but forces plasma to evaporate into the corona, as indeed EBTEL does.

## 4. Discussion and Conclusions.

Simple 0D hydrodynamic models have a long and quite successful history in modelling the temporal evolution of transiently-heated coronal loops. Motivated by discrepancies in some results, and by recent better understanding of coronal radiative cooling, we have updated our original version of the EBTEL model to include

gravitational stratification and correct radiative cooling. For the cases we have presented, we believe that the approximate model gives reasonable agreement with the full numerical results for the same parameters. EBTEL now permits highly over-dense loops to form in the cooling phase, and accounts for coronal stratification in long, cool loops. This is achieved through the evolution of the key parameter, the ratio of the transition region to coronal radiation. This is required to take on an equilibrium value around the time of maximum density, and a radiative value later on during the cooling. The transition is accomplished by either a linear or quadratic function. Our results suggest a slight preference for the linear one.

EBTEL is a useful tool in looking at the generic evolution of temperature and density, as well as the DEM of single loops. It runs fast (a few seconds on a contemporary laptop), and can be convolved with other software to generate, for example, light curves in various coronal emission lines, DEM profiles as a function of temperature etc. But, perhaps more useful is the ability to model a multi-strand corona. In such a scenario (e.g. Cargill, 1994; Cargill and Klimchuk, 1997), the coronal emission comes from many (perhaps thousands) of separately evolving strands. This is still beyond the abilities of 1D hydro codes, at least with a realistic turn-around time whereas EBTEL can model such a scenario in a few hours, and indeed perhaps less if a properly optimised version is used.

**Acknowledgements**

**Appendix. Comparison of analytical and numerical values of $C_1$ for a simple power law radiative loss function**

$C_1$ and $C_3$ can be calculated analytically from Martens (2010). Assuming uniform heating, a single power law slope of $\alpha$ for the radiation function, and boundary conditions of vanishing heat flux at top and bottom of loop, and vanishing temperature at bottom, he writes the energy equation in terms of the variable $\eta = (T/T_a)^{7/2}$ as:

$$\varepsilon \frac{d^2\eta}{ds^2} = \eta^\mu - \xi, \quad \mu = -\frac{2(2-\alpha)}{7}, \quad \xi = \frac{7}{3+2\alpha}, \tag{A1}$$

$$\varepsilon = \frac{2}{(1-2(2-\alpha)/7)}\left[\frac{2(2-\alpha)}{7}\right]^2 \frac{1}{B^2(\lambda+1,1/2)}, \quad \lambda = \frac{3/2+\alpha}{2(2-\alpha)}$$

where $T_a$ is the apex temperature and the scaling laws have been used to eliminate $L$, $Q$ and $p$. $B(a,b)$ is a beta function. Martens further solves the energy equation for a variable $u = \eta^{-\mu}$ as:

$$s/L = \beta_r(u, \lambda+1, 1/2),$$

where $\beta_r$ is the normalised incomplete beta function.

At the point where conduction changes from a gain to a loss, denoted by subscript zero, (A1) gives $\eta_0 = \left(\frac{7}{3+2\alpha}\right)^{-\frac{7}{2(2-\alpha)}}$ or, in real units, $\frac{T_0}{T_a} = \left(\frac{7}{3+2\alpha}\right)^{-\frac{1}{(2-\alpha)}}$.

Setting $\alpha = -1/2$, we get $C_3 = T_0/T_a = (2/7)^{2/5} = 0.606$. For $\alpha = -2/3$, $C_3 = 0.584$.

We can also calculate $C_1$ as follows. The dimensionless coronal radiative losses are:

$$\int_{s(\eta_0)}^{1} \eta^\mu ds = \xi(1-s(\eta_0)) - \varepsilon\left(\frac{d\eta}{ds}\right)_{s=s(\eta_0)}$$

Now Eq (A1) integrates once to give, on application of the boundary conditions:

$$\frac{\varepsilon}{2}\left(\frac{d\eta}{ds}\right)^2 = \frac{\eta^{\mu+1}}{\mu+1} - \xi\eta \tag{A2}$$

so that

$$\left(\frac{d\eta}{ds}\right)_{s=s(\eta_0)} = \sqrt{\frac{2}{\varepsilon}\left(\frac{\eta_0^{\mu+1}}{\mu+1} - \xi\eta_0\right)} \tag{A3}$$

The total radiative loss is just $\xi$ in these units so that the TR loss is then:

$$\int_0^{s(\eta_0)} \eta^\mu ds = \xi s(\eta_0) + \varepsilon \left( \frac{d\eta}{ds} \right)_{s=s(\eta_0)}$$

We have calculated $\eta_0$ above, and so can obtain $C_1$, which is independent of $Q$, $L$ and $p$. For $\alpha = -1/2$, we get $C_1 = 1.76$ and for $\alpha = -2/3$, $C_1 = 2.095$.

We now compare the Martens solutions with a numerical solution with a lower boundary at $2 \times 10^4$ K and a single power law loss function above $10^5$ K and a loss function scaling as $T^2$ below. [This eliminates the problem that the vanishing heat flux is only exactly enforceable in the limit of vanishing base temperature.] Care is needed with the grid on which the hydrostatic equations are solved. We used:

$$s/L = (2/\pi)\left| \sin^{-1}x - x\sqrt{1\text{-}x^2} \right|$$

where $x$ is evenly distributed between 0 and 1. 5000 points are used. The motivation for this grid can be seen from Eq (C1) of Rosner et al (1978) and it does give well-resolved solutions at all temperatures.

An array of cases has been run: three loop half-lengths, 2.5, 5 and 7.5 x $10^9$, and $T_a$ between $10^6$ and $10^7$ for each length. It turns out that the results are by and large independent of the loop half-length, so individual cases are not shown, rather the range of values found as shown in the following Table.

| $\alpha = -1/2.$ | $C_1$ | $C_2$ | $C_3$ |
|---|---|---|---|
| Analytic | 1.76 | 0.89 | 0.606 |
| Numerical | 1.65 – 1.74 | 0.895 | 0.62 – 0.61 |
| $\alpha = -2/3$ | | | |
| Analytic | 2.09 | 0.89 | 0.585 |
| Numerical | 1.88 – 2.06 | 0.892 | 0.61 – 0.59 |

**Table A1**. The constants $C_1$, $C_2$ and $C_3$ for two loss functions. The range of values in each box are those obtained as $T_a$ increases from low to high.

It can be seen that $C_2 = 0.9$ and $C_3 = 0.6$ are reasonable values for both cases. The lower values of $C_1$ correspond to smaller $T_a$ where the $T^2$ loss function at lower temperatures makes a greater relative contribution to the loop losses. We would argue that for a simple model, $C_1 = 1.7$ for $\alpha = -1/2$ and $C_1 = 2$ for $\alpha = -2/3$ are appropriate.

## References

Antiochos, S. K., Sturrock, P.A. 1978, ApJ, 220, 1137

Antiochos, S. K., MacNeice, P. J., Spicer, D. S., & Klimchuk, J. A. 1999, ApJ, 512, 985

Aschwanden, M. J., & Tsiklauri, D. ApJ Supp, 185, 171

Bradshaw, S. J., & Mason, H. E. 2003a, A&A, 401, 699

Bradshaw, S. J., & Mason, H. E. 2003b, A&A, 407, 1127

Bradshaw, S. J., & Cargill, P. J. 2005, A&A, 437, 311

Bradshaw, S. J., & Cargill, P. J. 2006, A&A, 458, 987

Bradshaw, S. J., & Cargill, P. J. 2010a, ApJ Lett., 710, L39

Bradshaw, S. J., & Cargill, P. J. 2010b, ApJ, 717, 163

Bradshaw, S. J., & Klimchuk, J. A. 2011, ApJ Supp, 194, 26

Cargill, P. J. 1994, ApJ 422, 381

Cargill, P. J., Mariska, J. T., & Antiochos, S. K., 1995, ApJ, 439, 1034

Cargill, P. J., & Klimchuk, J. A. 1997, 478, 799

Cargill, P. J., & Klimchuk, J. A. 2004, 605, 911

Cargill, P. J., Bradshaw, S. J. & Klimchuk, J. A., 2011, ApJ to be submitted.

Fisher, G. H., & Hawley, S. L. 1990, ApJ, 357, 243

Klimchuk, J. A., 2006, Solar Phys., 234, 41

Klimchuk, J. A., Antiochos, S. K., & Mariska, J. T. 1987, ApJ, 320, 409

Klimchuk, J. A., Patsourakos, S., & Cargill, P. J. ApJ, 682, 1351

Kopp, R. A., & Poletto, G. 1993, ApJ, 418, 496

Kuin, N. P. M., & Martens, P. C. H. 1982, A&A, 108, L1

McClymont, A. N., & Canfield, R. C., 1983a, ApJ 265, 483

McClymont, A. N., & Canfield, R. C., 1983a, ApJ 265, 497

Martens, P. C. H. 2010, ApJ, 714, 1290

Peres, G., 2000, Solar Phys., 193, 33

Rosner, R., Tucker, W. H. & Vaiana, G. S., 1978, ApJ, 220, 643

Serio, S., Peres, G., Vaiana, G. S., Golub, L., & Rosner, R. 1981, ApJ, 243, 288

Serio, S., Reale, F., Jakimiec, J., Sylwester, B., & Sylwester, J. 1991, A&A, 241, 197

Vesecky, J. F., Antiochos, S. K., & Underwood, J. H. 1979, ApJ, 233, 987

Warren, H. P., Brooks, D. H. & Winebarger, A. R., 2011, 734, 90

**Figure 1**: The upper two panels show $C_1$ as a function of $T_a$ for $L = 5 \ 10^9$ cm (left) and $7.5 \ 10^9$ cm (right) for a single power law loss function with a low temperature correction. Stars, circles and plus signs are, respectively, $C_1$ in absence of gravity, $C_1$ with gravity (both are from numerical solutions of the hydrostatic equations) and the estimate of $C_1$ in Eq (11). The lower two panels show the ratio of the radiative losses without gravity to those with gravity in the transition region (stars) and corona (circles). The ratio of the two transition region losses is roughly constant.

**Figure 2**: $C_1$ as a function of $T_a$ for $L = 5 \ 10^9$ cm. There is no gravity. In the left plot stars, circles and plus signs are, respectively, $C_1$ for single power loss function with low temperature correction, $C_1$ for the full EBTEL loss function, and the estimate of $C_1$ in Eq (12). The right column shows the ratio of radiative losses assuming a single power law and the full EBTEL form in the transition region (stars) and corona (circles).

**Figure 3**: The upper row shows $C_1$ as a function of $T_a$ for two temperature ranges and $L = 5 \ 10^9$ cm. Stars, circles and plus signs are, respectively, $C_1$ for single power loss function and no gravity, for the EBTEL loss function and gravity, and the estimate of $C_1$ in Eq (13). The lower row shows the ratio of radiative losses assuming a single power law with low temperature correction and no gravity, and the EBTEL loss function and gravity in the transition region (stars) and corona (circles).

**Figure 4.** The temperature and density (upper row) and $C_1$ (lower right panel) as a function of time for a nanoflare in a short ($L = 25$ Mm) loop. The lower left panel shows the relationship between $T$ and $n$, and the evolution can be tracked in time by going right along the horizontal lines at low density (the heating phase) and following the curves. The line coding is as follows: EBTEL-1 values of $C_{1-3}$ (dot), EBTEL-2 values of $C_{1-3}$ implemented as follows: EBTEL-2 with constant $C_1$ (dash-dot), linear $C_1$ model (dashed) and quadratic $C_1$ model (thin solid). The Hydrad results are shown by the thick solid lines. The small panel in the temperature plot shows its evolution in more detail around the maximum. In the $T$-$n$ plot, the straight solid lines are the scalings $T \sim n^2$ and $T \sim n^{1/2}$. $C_1$ is only shown for the linear and quadratic models and the gravitational and radiative corrections to $C_1$ are not included.

**Figure 5.** As Figure 4, but shows the effect of introducing radiative and gravity corrections to the $C_1$ model. The dotted curves show results for the quadratic $C_1$ profile in Figure 4, the dash-dot curve includes only the radiative correction and both radiative and gravitational corrections are shown for linear (dashed) and quadratic (solid) cases. The thick, solid curve is the Hydrad result.

**Figure 6.** The DEM for a nanoflare in a short ($L = 25$ Mm) loop. The left panel shows separate coronal and TR contributions. The dash-dot, dotted, solid and dashed lines are respectively the coronal DEM for (i) EBTEL-1 values of $C_{1-3}$, (ii) the quadratic $C_1$ profile without gravity and radiation corrections, and (iii) and (iv) quadratic and linear $C_1$ profiles with gravitational and radiative correction included. The thick dashed line is the transition region DEM associated with coronal DEM (iii). The right panel shows the sum of the coronal and TR DEMs for EBTEL-1 (dash-dot), EBTEL-2 with quadratic transition and radiative and gravity modifications (solid) and Hydrad (thick solid).

**Figure 7.** The results for a nanoflare in a long loop ($L = 75$ Mm). The figure format is the same as Figure 4. The curves are: EBTEL-1 (dash-dot), EBTEL-2 with (a) quadratic $C_1$ model (dots), (b) quadratic model with gravity and radiative correction (solid), (c) linear model with corrections (dashed) and Hydrad (thick solid).
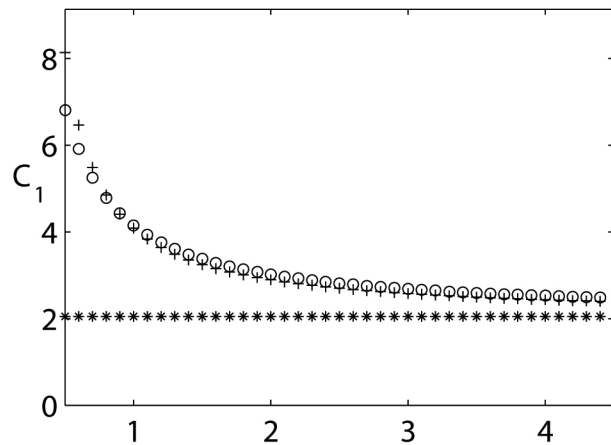
**Figure 8**. The DEM for a nanoflare in a long (75 Mm) loop. The line coding is as in Figure 6 except that the thick dash-dot line in the left panel is the TR DEM in the absence of the gravitational correction.

**Figure 9.** A nanoflare in a small loop with large initial density. The dash-dot, solid, dashed and thick solid curves show EBTEL-1, quadratic and linear $C_1$ profiles for EBTEL-2 and Hydrad.

**Figure 10** Temperature, density, $T$-$n$ and $C_1$ as a function of time for a small flare. The line coding is as follows: dash-dot (EBTEL-1), quadratic $C_1$ transition, no corrections (dots), quadratic and linear $C_1$ models with gravity and radiation (solid and dashed). Two Hydrad results are shown corresponding to the two chromospheric

radiation models in the text. The one where the radiation is limited above a density of $10^{12}$ cm$^{-3}$ is shown as the thick solid line in all panels, that where the radiation is limited above a density of $10^{11}$ cm$^{-3}$ is shown as the thick dashed line in the density plot.